# Observation of stable phase jump lines in convection of a twisted nematic

Soichi Tatsumi* and Masaki Sano

*Department of Physics, The University of Tokyo,*

*7-3-1 Hongo, Bunkyo-ku Tokyo,113-0033*

A. G. Rossberg

*Graduate School of Environment and Information Sciences,*

*Yokohama National University, 79-7 Tokiwadai, Hodogaya-Ku Yokohama 240-8501*



## Abstract

We report observations of stable, localized, line-like structures in the spatially periodic pattern formed by nematic electroconvection, along which the phase of the pattern jumps by $\pi$. With increasing electric voltage, these lines form a grid-like structure that goes over into a structure indistinguishable from the well known grid pattern. We present theoretical arguments that suggest that the twisted cell geometry we are using is indirectly stabilizing the phase jump lines, and that the PJL lattice is caused by an interaction of phase jump lines and a zig-zag instability of the surrounding pattern.

*Electronic address: tatsumi@daisy.phys.s.u-tokyo.ac.jp

## 1. INTRODUCTION

Usually, topological defects in the phase of periodic spatial modulations have co-dimension two. They are point-like in two dimensions, line-like in three dimensions, and in one dimension they reduce, for dynamical systems, to short events, localized in space and time[1]. Here we report the observation of stable, self-organized phase defects that extend to line-like objects in 2d: *Phase jump lines* (PJL) stretched parallel to the wavevector of the modulation, characterized by a change of the phase of the spatial modulation by $\pi$ on a short distance (Fig.1).

The phenomenon was observed in the periodic pattern of convection rolls forming in thin layers of the nematic liquid crystal MBBA (4-methoxybenzylidene-4'-butylaniline) under the influence of an electric ac field ($\|\hat{z}$) that is oriented normal to the ($x$-$y$) layer and the alignment of the nematic director. Electroconvection (EC) in nematic liquid crystals has been studied extensively. After early studies by E. Dubois-Violette and others [2] aimed at understanding the basic mechanism of convection, EC later became popular as a model for pattern formation in anisotropic systems. Depending on the experimental conditions, the convection rolls are aligned either preferentially normal to the symmetry axis ($\hat{x}$) of the system—defined by the direction at which the nematic director is anchored at the boundaries—or oblique at some preferred angel. In the oblique-roll case, two convective modes related to each other by a reflection at the $x$ axis coexist [3, 4]. Near the onset of convection, descriptions in terms of one (normal rolls) or two (oblique rolls) time-dependent Ginzburg-Landau equations could be established [5]. These equations are of potential type and predict a relaxation to a simple equilibrium state.

The more puzzling was the rich dynamics of the system observed for stronger electric fields, with scenarios such as those named "fluctuating Williams domains", "chevron patterns", "abnormal rolls", "grid patterns", or "defect lattices" being reported [6, 7, 8, 9, 10, 11, 12, 13, 14, 15, 16, 17, 18]. Only in recent years it became clear that most of these observations can be understood by the non-relaxational interaction of the convective mode(s) with only one additional, weakly damped mode that describes an in-plane rotation of the nematic director. A Ginzburg-Landau-type model for the non-relaxational coupling of these two (or three) modes, called *standard model* below, explains most of the experimentaly observed scenarios at least qualitatively, and predicts a few more [19, 20].

There are several indications in the literature that hint at the existence of stable PJL in nematic electroconvection. For example, for the defect-chaotic regime of normal rolls called "fluctuating

Williams domains" it is well known that the "shape" of topological defects, particularly near the events of defect creations and annihilations, can be highly anisotropic. Their extension in $x$ direction is considerably larger than in $y$ direction. As such this deformation could be explained by the anisotropy of the linear dispersion relation of the convective mode, which can be removed by a simple rescaling of the $x$ axis. But in some cases the defects stretch considerably and are then more naturally characterized as "phase jump lines" [21, 22, 23]. These structures seem to be related to weakly unstable saddles corresponding to the stable PJL reported here. Stable PJL have also been seen in numerical simulations of the standard model [24]. Yet, a general theory is missing, and it remains unclear if or under which conditions stable PJL would be observable in electroconvection.

In our experiments, the conventional EC setup was modified by twisting the nematic within the layer: Instead of anchoring the nematic director at the surfaces of the layer parallel to the $x$ axis, the anchoring direction is rotated by a fixed angle in opposite directions at the two surfaces [25, 26, 27, 28]. This geometry seems to be favorable for PJL.

In the following we first describe the details of the twisted EC setup, and describe the observed PJL and structures they form. We then discuss some theoretical ideas that understanding these observations.

## 2. EXPERIMENTAL SETUP

The nematic liquid crystal MBBA doped with 0.1wt% tetra-n-butylammonium bromide to stabilize the conductivity was sandwiched between two glass plates covered with transparent indium tin oxide thin-film electrodes. The lateral extensions of the liquid crystal layer were $2\mathrm{cm} \times 2\mathrm{cm}$ and its thickness $d = 50\mu\mathrm{m}$. The surfaces of the plates were coated with polyvinyl alcohol and rubbed in order to attain a planar anchoring of the nematic molecules. Temperature of the cell was controlled at $25 \pm 0.01$ ℃. A standard wave-generator was used to apply ac voltages $V = \mathcal{O}(100\mathrm{V})$ of frequencies $f$ up to several $\mathrm{kHz}$ to the electrodes. The structure of the cell is shown schematically in Fig. 1. The anchoring direction for each plate is represented by an arrow. By rotating the anchoring direction by an angle $\alpha = \pi/4$ out of the $x$ axis at the lower plate, and in opposite direction by the same amount at the upper plate, the nematic director is twisted along the $z$-axis in the ground state [40] (Fig. 1).

## 3. EXPERIMENTAL RESULTS

The control parameters of the system are the externally applied voltage and its frequency. A phase diagram of the observed patterns is shown in the Fig. 2. The cutoff frequency $f_c$, where the conductive mode of electroconvection is superseded by the dielectric mode, was above $1\,\mathrm{kHz}$. Measurements were performed for $f < f_c$, *i.e.*, in the conductive regime. As the voltage was increased, normal rolls with a wavevector parallel to the $x$-axis (at an angle of $\alpha$ to each anchoring direction) were observed. Besides the well-known states including normal rolls (parallel rolls), grid pattern (rectangular cells), and dynamic scattering modes (3D turbulent states), we found stably aligned phase jump lines (PJL) in a wide frequency range of the conductive regime.

Figures 3a-c show the shadow-graph image of PJL observed under a polarization microscope (polars $\| \; x$). PJL can have finite length. At the endpoints of PJL the phase difference between the adjacent domains gradually decreases to zero. As the voltage is increased, the typical distance $L$ between PJL in $y$ direction decreases.

In order to determine $L$, which is below expressed in terms of the wave number $K := 2\pi/L$, quantitatively, two methods were employed. The first makes direct use of the Fourier transforms of recorded images (Figs. 3b',c'). The other method is to count the number $n$ [41] of PJL along a line of length $E$ parallel to $\hat{y}$, which gives $K = 2\pi n/E$. For high voltage, the Fourier analysis was preferred. At lower voltages we used the counting method, since the small number of PJL would not lead to sharp peaks in the Fourier transform. We verified that in the intermediate range the results of the two methods coincide.

In Fig. 4 the measured wave number $K$ is plotted against the normalized distance $\epsilon = (V^2 - V_c^2)/V_c^2$ from the threshold of convection $V_c$. The data indicate that $K$ goes to zero following a square-root law

$$K = c\,(\epsilon - \epsilon_1)^{1/2} \tag{1}$$

with $\epsilon_1 > 0$. For $f = 400\mathrm{Hz}$ we obtain $c = 50.5\mathrm{mm}^{-1}$ and $\epsilon_1 = 0.22$ and for $f = 600Hz$ data is well described by $c = 95.3\mathrm{mm}^{-1}$ and $\epsilon_1 = 0.31$.

Some observations indicate that there are at least two different regimes of PJL. At low $\epsilon$, the spacing between PJL is very irregular (Fig. 3a,b) and the PJL continue to move, although very slowly. At high $\epsilon$, where the spacing between PJL is smaller, it becomes also more regular (as can be seen from the sharp peaks in the Fourier transform of Fig. 3c shown in Fig. 3c'), and a

steady state is reached. We refer to the resulting structure as a *PJL grid*. The onset voltage of PJL grids is well above the onset of PJL (Fig. 2). At this point the $K$ *vs* $\epsilon$ relation also starts to deviate significantly from the square-root law valid for smaller $\epsilon$, as shown in Fig. 4. The deviation is towards larger $K$, i.e. towards denser PJL, contrary to what one would expect from a repulsive interaction between PJL. The PJL grids are visually indistinguishable from the well-known grid pattern[29] consisting of two overlapping sets of oblique rolls. If the two structures are indeed identical this means that we found a new route from normal rolls to oblique rolls, different from the conventional transition *via* a zig-zag instability. But further investigations are required to confirm this hypothesis. For the low-$\epsilon$ range, on the other hand, some first steps towards a better understanding have been made.

## 4. THEORY

A clear theoretical picture of PJL, including the conditions for their existence as well a description of their interaction with the surrounding roll pattern and with each other, has not yet emerged. Even though other mechanisms leading to stable PJL appear to exist [30], the simulations of Zhao [24] strongly suggest that the observed PJL can be described by the standard model for normal-roll electroconvection. We shall here investigate three aspects related to this problem that help understanding why PJL stabilize in twisted cells and how they are forming PJL grids.

The standard model [19, 20, 31, 32, 33] is given by

$$\begin{aligned}\tau\partial_t A =& i\beta A\partial_y\phi + \Big(\epsilon + \xi_x^2\partial_x^2 + \xi_y^2\partial_y^2 \\ &+ 2iq_c\,\xi_y^2\,C_1\phi\partial_y - C_2 q_c^2\xi_y^2\phi^2 - g|A|^2\Big)A,\end{aligned} \tag{2a}$$

$$\begin{aligned}\gamma_1\partial_t\phi =& -h\phi + K_3\partial_x^2\phi + K_1\partial_y^2\phi \\ &+ 2\Gamma\,\mathrm{Im}\{A^*(\partial_y - iq_c\phi)A\}.\end{aligned} \tag{2b}$$

It describes the interaction of two spatio-temporally slow variables: The complex amplitude $A$ of the convection pattern $\sim (Ae^{iq_c x} + \text{c.c.})$, and the amount $\phi$ of in-plane rotation of the nematic director. By the requirements of structural stability and according to theoretical and experimental results for the untwisted geometry, the time-constants $\tau$ and $\gamma_1$, the coherence lengths $\xi_x$, $\xi_y$, the critical wave number $q_c$, the geometry factors $C_1$ and $C_2$, the Landau coefficient $g$, the damping constant $h$, and the two elastic constants $K_1$ and $K_3$ are all positive. The sign of $\beta$ depends on the applied frequency and the experimental geometry and is difficult to determine *a priori*. The value

of $\Gamma$ is always found to be negative and we shall assume this hereafter. It is easily seen that with negative $\Gamma$ convection rolls ($A \neq 0$) have a destabilizing effect on $\phi$. This effect is crucial for most of the complex patterns observed in electroconvection, and PJL are no exception.

### 4.1. Stabilization of PJL

After scaling out the natural $\epsilon$ dependence of $A$, $\phi$ and length and time scales ($\partial_x \sim \partial_y \sim A \sim \phi \sim \epsilon^{1/2}$, $\partial_t \sim \epsilon$), the standard model (2) can be reformulated by the following, equivalent system of PDE:

$$\tau \partial_t A = (1 + \partial_x^2 + \partial_y^2 + 2i\, C_1 \phi \partial_y - C_2 \phi^2 - |A|^2) A + i\beta A \partial_y \phi, \tag{3a}$$

$$\partial_t \phi = -\, h\, \phi + \partial_y^2 \phi + K_3 \partial_x^2 \phi - 2|\Gamma|\, \mathrm{Im}\{A^* (\partial_y - i\phi) A\}. \tag{3b}$$

The coefficients and variables in system (3) are not identical to those denoted with the same symbols in system (2), but are related to these by simple scaling transformations. For all coefficients but $h$ this relation is independent of $\epsilon$. The coefficient $h$ in Eq. (3b) scales as $\epsilon^{-1}$, i.e., $h$ plays the role of the main control parameter in the rescaled equations (3). As $h$ decreases, the first instability of the homogeneous solution $A = 1$, $\phi = 0$ is to abnormal rolls at $h = 2|\Gamma|$ if $\beta < 0$ and to zig-zag modulations at $h = 2|\Gamma|(1 + \beta)$ if $\beta > 0$.

The system also has a steady-state solution

$$\phi = 0, \quad A = \tanh\left(y/\sqrt{2}\right) \tag{4}$$

that describes PJL. For large $h$, i.e. close to the threshold of convection, PJL are unstable. This can be seen by considering the limit $h \to \infty$ where $\phi = 0$ is fixed. Then solution (4) is unstable to the linear mode $\delta A = i\, \mathrm{sech}(y/\sqrt{2})$ with growth rate $\tau^{-1}$ [34]. However, by lowering $h$ the additional degree of freedom $\phi$ can stabilize the PJL by an interaction through the last term in Eq. (3b). For a discussion of this process, we linearize the system (3) with respect to perturbations of solution (4) of the form $\delta A = [a_r(y) + i a_i(y)] \exp(\sigma t)$, $\delta\phi = f(y) \exp(\sigma t)$, which leads to

$$0 = \left( -\sigma\, \tau + 1 - 3 \tanh^2 \frac{y}{\sqrt{2}} + \partial_y^2 \right) a_r, \tag{5}$$

and

$$0 = \left(-\sqrt{2}\, C_1 \,\mathrm{sech}^2 \frac{y}{\sqrt{2}} + \beta \,\tanh \frac{y}{\sqrt{2}}\, \partial_y\right) f + \left(-\sigma\, \tau + \mathrm{sech}^2 \frac{y}{\sqrt{2}} + \partial_y^2\right) a_i, \tag{6a}$$

$$0 = \left(-\sigma - h - 2|\Gamma| \tanh^2 \frac{y}{\sqrt{2}} + \partial_y^2\right) f - \left(\sqrt{2}\,|\Gamma| \mathrm{sech}^2 \frac{y}{\sqrt{2}} - 2\,|\Gamma|\, \tanh \frac{y}{\sqrt{2}} \partial_y\right) a_i. \tag{6b}$$

We are looking for eigenfunctions of these equations which are bounded for $y \to \pm\infty$. Equation (5) is decoupled from Eqs. (6a,6b). Apart from the translational mode $a_r = \partial_y \tanh(y/\sqrt{2})$, Eq. (5) has bounded solutions only with $\tau\sigma \leq -3/2$ and does not contribute to the linear stability problem. The $y$ axis can be divided into an inner region $|y| \lesssim 5$ near the PJL, and two outer regions where the system (6) simplifies. For $y > 0$, for example, the substitutions $\mathrm{sech} \to 0$, $\tanh \to 1$ lead to

$$0 = (-\sigma\tau + \partial_y^2) a_i + \beta \partial_y f, \tag{7a}$$

$$0 = (-\sigma + 2|\Gamma|\mu + \partial_y^2) f - 2|\Gamma| \partial_y a_i, \tag{7b}$$

where we introduced the abbreviation $\mu = 1 - h/2|\Gamma|$. In general, the eigenmodes of Eq. (6) have to be calculated numerically. For example this can be done by "shooting" solutions starting at $y = 0$ with $a_i = 1$, $f = f_0$, $a_i' = f' = 0$ into the $y > 0$ outer region such as to match $a_i(y_1), a_i'(y_1), f(y_1), f'(y_1)$ for sufficiently large $y_1$ with a bounded outer solution. We shall here only be interested in the cases where the PJL stabilize prior to any destabilization of the homogeneous state, i.e., for the cases that $\mu < -\beta$ and $\mu < 0$. The bounded outer solutions are then generally given by linear combinations of the two solutions of (7) of the form $a_i, f \sim \exp(\lambda y)$ with $\lambda \leq 0$ and

$$\lambda^2 = \frac{\mu\sigma\tau}{\beta + \mu} + \mathcal{O}(\sigma^2) \tag{8}$$

or

$$\lambda^2 = -\,2|\Gamma|\,(\beta + \mu) + \mathcal{O}(\sigma), \tag{9}$$

respectively. The value of $\mu$ where the PJL stabilize can be found by considering the limit $\sigma \to 0^+$ of the systems (6) and (7). Two particularities of this limit will be used here: (i) The outer solution

corresponding to (8) goes over into a simple phase shift ($f = 0$, $a_i = $ const.). Thus, $f$ contains only contributions from the component corresponding to (9) and must satisfy

$$\partial_y f = -\sqrt{-2|\Gamma|(\beta + \mu)}\, f. \tag{10}$$

(ii) By Eq. (7a) the quantity

$$u = \partial_y a_i + \beta f \quad (= 0) \tag{11}$$

is conserved along $y$ in the outer region [24]. When $\mu < -\beta$ and (10) holds, this implies $u = 0$ for bounded solutions. Equations (10,11) are necessary and sufficient conditions for the inner solutions to be bounded when continued to $y \to \infty$. When the shooting method is used, the two conditions can be satisfied by adjusting the initial value $f_0$ of $f$ at $y = 0$ and the value of the control parameter $\mu$.

With $C_1 > 1$ we could find neutrally stable modes of PJL with $\mu < -\beta$ for all parameter sets tested, in particular for positive as well as negative $\beta$. For example, Fig. (5) shows the neutrally stable mode of the PJL for parameters $\Gamma = -0.6$, $\beta = 0.3$, $C_1 = 1.1$, and $\tau = 0.5$. These parameters are suggested by numerical calculations for similar systems [31]. For this case we verified that there is no unstable mode, i.e., Fig. (5) shows the critical mode of a PJL. (For smaller $|\Gamma|$, e.g. with $\Gamma = -0.06$, there is another mode with positive growth rate. Then the feed-back loop through $\phi$ is too weak to stabilized the PJL.)

As $C_1$ is lowered, the critical $\mu$ approaches $-\beta$ and the decay of the $f$ component in the far field becomes flatter, as described by Eq. (10). Thus $a_i$ increases/decreases approximately linearly over a wide range according to (11). For $\mu \to -\beta$, one expects the critical mode to converge to an unbounded secular solution with constant $\partial_y a_i$ and $f$ in the outer range.

It turns out that for $C_1 = 1$ the linearized equations (6) have the analytic solution

$$f = 1, \quad a_i = \sqrt{2}\,(1 - \mu) + \mu\, y\, \tanh \frac{y}{\sqrt{2}}. \tag{12}$$

For $\mu = -\beta$ this solution satisfies conditions (10) and (11) and is of the expected form. Combined with our numerical calculations, we conclude that the critical $\mu$ reaches $-\beta$ exactly when $C_1 = 1$. Thus, for $\beta_y > 0$, the PJL can stabilize prior to the zig-zag instability at $\mu = -\beta$ only if $C_1 > 1$.

For $\beta < 0$ the first instability of the homogeneous state and the far field in system (6) is towards abnormal rolls at $\mu = 0$. In contrast to the zig-zag instability at $\mu = -\beta$, the outer equations (7) have for $\mu = 0$ no secular solutions with $\sigma = 0$. Instead, the solution space corresponding

to $\lambda = 0$ [Eq. (8)] is spanned by two linearly independent constant solutions, the pure phase shift $(a_i, f) = (1, 0)$ and the pure director rotation $(a_i, f) = (0, 1)$. Since both are bounded, bounded solutions of (6) for $\mu = 0$ are obtained whenever the contribution to the outer solutions corresponding to Eq. (9) with $\lambda > 0$ vanishes. When the shooting method is used, this can be achieved by adjusting a single parameter, e.g. $f_0$. Thus, at the abnormal-roll instability $\mu = 0$, a neutrally stable linear mode of the PJL can always be found.

By the interaction of $f$ and $a_i$ in the core region, a certain linear combination of the constant outer modes is singled out, characterized by a specific ratio $r = a_i/f$ (for $y \to +\infty$). When $C_1 = 1$, for example, the analytic solution (12) gives $r = \sqrt{2}$. A perturbative analysis of the outer equations (6) for small $\sigma \sim \partial_y \sim \mu$ under the constraint $a_i/f = r + \mathcal{O}(\mu)$ yields a solution with $a_i, f \sim \exp(\lambda_s y)$ (as $y \to +\infty$) where

$$\lambda_s = \frac{2r\tau|\Gamma|\mu}{2r^2|\Gamma|\tau - \beta} + O(\mu^2) \tag{13a}$$

with the growth rate

$$\sigma = \frac{2\beta|\Gamma|\mu}{2r^2|\Gamma|\tau - \beta} + O(\mu^2). \tag{13b}$$

When $\lambda_s < 0$ this solution is bounded and an eigenmode of the PJL. Since $\sigma/\lambda_s = \beta/r\tau + \mathcal{O}(\mu^2)$, this mode can be stable only for $r < 0$, which is the case only for values of $C_1$ much smaller or much larger than one. Usually one would assume $r > 0$. With $-2|\Gamma|\, r^2\, \tau < \beta < 0$, for example, (13) then describe an unstable linear mode that becomes neutrally stable as $\mu$ approaches zero from below.

In conclusion, these considerations show that within the framework of the model (3) a stabilization of PJL of the form (4) prior to any destabilization of the homogeneous state—as we seem to observe it in the experiments—is possible, but likely only for $C_1 > 1$ and $\beta \gtrsim 0$.

### 4.2. The effect of the twisted anchoring on $C_1$

In order to test if the twisted anchoring used in our experiment can cause a higher value of $C_1$, we analyzed a model for the $z$ dependence of director twist $\hat{\phi}(z)$ and convection mode $\hat{A}(z)$ and their interaction [30, 35]. Keeping only terms that are relevant for determining $C_1$, the model reads

in appropriate dimensionless units

$$\tau\partial_t\hat{A} = \left[u - (P-\hat{\phi})^2 + \partial_z^2\right]\hat{A} \tag{14a}$$

$$\partial_t\hat{\phi} = \partial_z^2\hat{\phi} + 2\Gamma|\hat{A}|^2(P-\hat{\phi}). \tag{14b}$$

The coefficient $u$ in Eq. (14a) is a control parameter that depends on the applied voltage. $P$ corresponds to the angle of the wavevector of a plane-wave convection mode to the $x$ axis and the term $-(P-\hat{\phi})^2$ in Eq. (14a) describes the preference of the convective modes to align normal to the director. The last term ($\partial_z^2$) describes the diffusion of hydrodynamic variables along $z$. In Eq. (14b) the first term describes the stiffness of the in-plane director to twist and the second term the torque generated by misaligned rolls on the director. We assume layers of thickness $2$ without loss of generality and impose the boundary conditions $\hat{A}(\pm 1) = 0$ and, corresponding the twisted anchoring, $\hat{\phi}(+1) = b$, $\hat{\phi}(-1) = -b$. The isotropy of the system is broken only by the boundary condition. In the bulk, isotropy is preserved, which is reflected by the equivariance under $P \to P + \delta$, $\hat{\phi} \to \hat{\phi} + \delta$. The model can be derived analytically in the limit that the wavelength of the roll pattern is much smaller than the layer thickness [30]. However, since this condition is not satisfied for our experimental system, we expect the model to describe the experiment only qualitatively.

The coefficient $C_1$ entering the 2d description (3) can be obtained by the following method. Noting that in the basic state ($\hat{A} = 0$) the director relaxes to $\hat{\phi} = bz$, and that the fundamental mode of linear excitations of $\hat{\phi}$ is $\hat{\phi}_1 = \cos(\pi z/2)$, we assume a weakly excited $\hat{\phi} = bz + K\hat{\phi}_1$ and search numerically for the threshold value $u_{\text{crit}}$ of the control parameter $u$ at which the lowest eigenmode $\hat{A}(z) = \hat{A}_{\text{crit}}(z)$ of Eq. (14a) becomes critical ($\partial_t = 0$). The orientation $P$ of the roll wavevector is chosen such as to minimize $u_{\text{crit}}$. This corresponds to letting $A = \exp(iPy)$ in Eq. (3a) with $P = C_1\phi$. Following general prescriptions (e.g. [36, 37]), the value of $C_1$ is then given by the ratio of projections of two components of the r.h.s. of Eq. (14b) onto its adjoint eigenvector ($\equiv \hat{\phi}_1$)

$$C_1 = \frac{\displaystyle\int_{-1}^{1} \hat{\phi}_1\, 2\Gamma|\hat{A}|^2 P\, dz}{\displaystyle\int_{-1}^{1} \hat{\phi}_1\, 2\Gamma|\hat{A}|^2\hat{\phi}\, dz} \tag{15}$$

in the limit $K \to 0$.

Without twist ($b = 0$) we reproduce the analytic result [42] $C_1 = 256/(27\pi^2) = 0.96$ [30, 38]. With increasing twist $b$, the value of $C_1$ increases, until it reaches a maximum $C_1 = 1.14$ at $b = 8.1$

(Fig. 6). The result is independent of all other system parameters. Due to the purely geometric nature of this effect, it is plausible to assume that the twist leads to an increased value of $C_1$ also in our experimental system.

### 4.3. Coupling to zig-zag modulations

Simulations [24] show that PJL can also coexist with zig-zag modulations of the roll pattern. The PJL are then located at preferred phase angles of the zig-zag modulation. Thus, the distance $L$ between neighbouring PJL will be controlled by the wavelength $\Lambda$ of the zig-zag modulation. Even though they are not clearly visible in the experiments, small zig-zag modulations are probably also controlling the distance between PJL in PJL grids.

To test this hypothesis, the wavelength of zig-zags is estimated. For an easy comparison with experiments, dimensional units are used in this calculation. In the absences of strong variations of the pattern amplitude $|A|$, the dynamics of the roll pattern can be described in terms of the phase $\theta = \arg A \,(\mathrm{mod}\, 2\pi)$ of the pattern alone. Together with the coupling to $\phi$, this is description becomes [32, 39]

$$\tau\partial_t\theta = \xi_x^2\partial_x^2\theta + \xi_y^2\partial_y^2\theta + \beta\partial_y\phi + r\phi^2\partial_y\phi, \tag{16a}$$

$$\gamma_1\partial_t\phi = 2|\Gamma|(\epsilon - \epsilon_{\mathrm{AR}})\phi - g\phi^3 + K_3\partial_x^2\phi + K_1\partial_y^2\phi - 2|\Gamma|\epsilon\partial_y\theta \tag{16b}$$

with positive $r, g$, the threshold of abnormal rolls $\epsilon_{\mathrm{AR}} = h/(2|\Gamma|)$ and all other parameters identical to those entering Eq. (2). While the derivation of the nonlinear terms in this system hinges on the assumption of that spatial and temporal variations of $\theta$ and $\phi$ are slow on the scales $\xi_{x,y}\epsilon^{-1}$ and $\tau\epsilon^{-1}$, which is strictly satisfied only for small $\epsilon - \epsilon_{\mathrm{AR}}$ and $\beta$, the linear part is valid uniformly in $\epsilon \leq 0$ and $\beta$, as long as the Ginzburg-Landau description (2) is valid.

For stationary solutions that depend only on $y$ ($\partial_t, \partial_x = 0$) Eq. (16a) can be integrated to

$$\xi_y^2\partial_y\theta + \beta\phi + r\phi^3/3 = J = \text{const.} \tag{17}$$

In the simple case that rolls are not tilted on the average ($\langle\partial_y\theta\rangle_y = 0$) the integration constant $J$ vanishes. Using Eq. (17) to eliminate $\theta$ from Eq. (16b) then yields an equation for $\phi$ of the form [39]

$$K_1\partial_y^2\phi = -2|\Gamma|((1 + \beta/\xi_y^2)\epsilon - \epsilon_{\mathrm{AR}})\phi + g'(\epsilon)\phi^3. \tag{18}$$

While the wavelength of zig-zag modulations can become arbitrary large when the nonlinearity in Eq. (18) becomes effective, the wavelength of small-amplitude modulations is sharply determined as

$$\begin{aligned}\Lambda =&2\pi\sqrt{\frac{K_1}{2|\Gamma|((1+\beta/\xi_y^2)\epsilon-\epsilon_{\mathrm{AR}})}}\\ =&2\pi\sqrt{\frac{K_1\epsilon_{\mathrm{ZZ}}}{2|\Gamma|\epsilon_{\mathrm{AR}}(\epsilon-\epsilon_{\mathrm{ZZ}})}}.\end{aligned} \tag{19}$$

where $\epsilon_{\mathrm{ZZ}}=\epsilon_{\mathrm{AR}}/(1+\beta/\xi_y^2)$ denotes the threshold of the zig-zag instability. In order to estimate the value of $2|\Gamma|\epsilon_{\mathrm{AR}}/K_1$, recall that the linear part of Eq. (16b) holds also for $\epsilon=0$ (no convection). In this case the relaxation of small in-plane rotations of the director is easily described by the linearized Leslie-Erickson equations. For the untwisted case, for example, they reduce to

$$\gamma_1\partial_t n_y=(k_{33}\partial_x^2+k_{11}\partial_y^2+k_{22}\partial_z^2)n_y. \tag{20}$$

Considering only the slowest mode of the system for fixed boundary conditions at $z=\pm d/2$, $n_y=\phi\cos(\pi z/d)$, and projecting onto the corresponding adjoint $\cos(\pi z/d)$, yields

$$\gamma_1\partial_t\phi=(k_{33}\partial_x^2+k_{11}\partial_y^2-k_{22}\frac{\pi^2}{d^2})\phi. \tag{21}$$

Comparing of Eqs. (16b) and (21) shows that $2|\Gamma|\epsilon_{\mathrm{AR}}/K_1=\pi^2k_{22}/d^2k_{11}$. For MBBA at 25°C, for example, the ratio $k_{11}/k_{22}$ is $\approx 1.6$. For the twisted geometry one would expect some mixture of $k_{11}$, $k_{22}$, and $k_{33}$ to enter $K_1$ instead of just $k_{11}$, but since in the projection onto the adjoined mode the central part $z\approx 0$ dominates, and there the director is still aligned parallel to $\hat{x}$, these corrections are presumably small. Assuming a relation $L=m\,\Lambda$ between zig-zag wavelength $\Lambda$ and PJL distance $L$, one obtains the result

$$\begin{aligned}L=&2dm\sqrt{\frac{k_{11}\epsilon_{ZZ}}{k_{22}(\epsilon-\epsilon_{ZZ})}}.\\ \Leftrightarrow K=&\frac{\pi}{dm}\sqrt{\frac{k_{22}}{k_{11}}\frac{\epsilon-\epsilon_{ZZ}}{\epsilon_{ZZ}}}.\end{aligned} \tag{22}$$

Even when $\epsilon_{\mathrm{ZZ}}$ is fitted from the measured data for $K$, Eq. (22) makes a nontrivial prediction because $\epsilon_{\mathrm{ZZ}}$ appears at two different positions in the formula.

Using the fitted experimental curves, we find that Eq. (22) holds with $m=2.1$ for the $400\,\mathrm{Hz}$ data and with $m=0.94$ for the $600\,\mathrm{Hz}$ data. That is, in both cases we find a value of $m$ of order one. In view of the coarseness of the theoretical estimates, and allowing for some experimental

error, we conclude that the observations fully supports the hypothesis that the lattice constant of the PJL-grid is controlled by small zig-zag modulations. The mechanism by which the amplitude of zig-zag modulations or, equivalently, the zig-zag wavelength is kept small remains unclear, however.

## 5. CONCLUSION

In this study, we reported the observation of stable PJL and described a process by which these PJL from a lattice that finally evolves to a structure indistinguishable from the well know grid pattern as the applied voltage increases. We argued that the stabilization of PJL is presumably an indirect effect of the twisted geometry of the nematic in the basic state: The twist leads to values of the coefficient $C_1 > 1$, which in turn enables the stabilization of PJL prior to a destabilization of the roll pattern.

---


[1] A. J. Bray, Adv. Phys. **43**, 357 (1994).

[2] E. Dubois-Violette, G. Durand, E. Guyon, P. Manneville, and P. Pieransk, in *Solid state physics, Suppl. 14*, edited by L. Liebert (Academic Press, New York, 1978), p. 147.

[3] W. Zimmermann and L. Kramer, Phys. Rev. Lett. **55**, 402 (1985).

[4] E. Bodenschatz, W. Zimmermann, and L. Kramer, J. Phys. (Paris) **49**, 1875 (1988).

[5] L. Kramer and W. Pesch, Annu. Rev. Fluid Mech. **27**, 515 (1995).

[6] S. Kai, N. Chizumi, and M. Kohno, Phys. Rev. A **40**, 6554 (1989).

[7] H. Amm, R. Stannarius, and A. G. Rossberg, Physica D **126**, 171 (1999).

[8] J.-H. Huh, Y. Hidaka, A. G. Rossberg, and S. Kai, Phys. Rev. E **61**, 2769 (2000).

[9] A. G. Rossberg and L. Kramer, Physica D **115**, 19 (1998).

[10] S. Nasuno, M. Sano, and Y. Sawada, J. Phys. Soc. Jpn. **58**, 1875 (1989).

[11] M. Sano, K. Sato, S. Nasuno, and H. Kokubo, Phys. Rev. A **46**, 3540 (1992).

[12] S. Nasuno, N. Yoshimo, and S. Kai, Phys. Rev. E **51**, 1598 (1995).

[13] M. Dennin, D. S. Cannell, and G. Ahlers, Phys. Rev. E **57**, 638 (1998).

[14] R. Ribotta, A. Joets, and L. Lei, Phys. Rev. Lett. **56**, 1595 (1986).

[15] M. A. Scherer and G. Ahlers, Phys. Rev. E **65**, 051101 (2002).

[16] S. Rudroff, V. Frette, and I. Rehberg, Phys. Rev. E **59**, 1814 (1999).

[17] S. Sasa, Prog. Theor. Phys. Lett. **83**, 824 (1990).

[18] M. Oikawa, Y. Hidaka, and S. Kai, Jour. Phys. Soc. Jpn **73**, 2917 (2004).

[19] A. G. Rossberg, Dissertation, Universität Bayreuth (1997), URL `http://www.rossberg.net/ag/dissertation`.

[20] S. Komineas, H. Zhao, and L. Kramer, Phys. Rev. E **67**, 031701 (2003).

[21] S. Sasa, T. Mizuguchi, and M. Sano, Europhys. Lett. **19**, 593 (1992).

[22] Á. Buka, T. Börzsönyi, N. Éber, and T. Tóoth-Katona, Lecture Notes in Physics **567**, 298 (2001).

[23] P. E. Cladis, *Chirality in Liquid Crystals* (Springer, New York, 2001).

[24] H. Zhao, Ph.D. thesis, Universität Bayreuth (2000).

[25] A. Hertrich, A. P. Krekhov, and O. A. Scaldin, J. Phys. **4**, 239 (1994).

[26] H. Bohatsch and R. Stannarius, Phys. Rev. E **60**, 5591 (1999).

[27] A. G. Rossberg, Phys. Rev. E **62**, 4682 (2000).

[28] V. A. Delev, P. Toth, and A. P. Krekhov, Mol. Cryst. and Liq. Cryst. **351**, 179 (2000).

[29] S. Kai, N. Yashitsune, and K. Hirakawa, J. Phys. Soc. Jpn. **40**, 267 (1976).

[30] A. G. Rossberg, Phys. Rev. E **62**, 8114 (2000).

[31] A. G. Rossberg, A. Hertrich, L. Kramer, and W. Pesch, Phys. Rev. Lett. **76**, 4729 (1996).

[32] S. Rudroff, H. Zhao, L. Kramer, and I. Rehberg, Phys. Rev. Lett. **81**, 4144 (1998).

[33] W. Zimmermann, Ph.D. thesis, Universität Bayreuth (1988).

[34] J. S. Langer and V. Ambegaokar, Phys. Rev. **164**, 498 (1967).

[35] A. G. Rossberg, Phys. Rev. E **62**, 4682 (2000).

[36] P. Manneville, *Dissipative Structures and Weak Turbulence* (Academic Press, New York, 1990).

[37] A. Buka and e. L. Kramer, *Pattern formation in liquid crystals* (Springer-Verlag, New York, 1995).

[38] A. Lindner, Diploma thesis, Universität Bayreuth (1997).

[39] H. Zhao and L. Kramer, Phys. Rev. E **62**, 5092 (2000).

[40] This geometry allows two equivalent ground states: left twist and right twist. For the experiments a region of the sample without domain walls (uniform twist) was selected.

[41] The number $n$ averaged over a full image was determined by first summing the $x$-extension of all PJL in the image and dividing this number by the $x$-width of the image.

[42] This result does not depend on the absence or presence of flexoelectric effects, as a note in Ref. [20] might suggest.

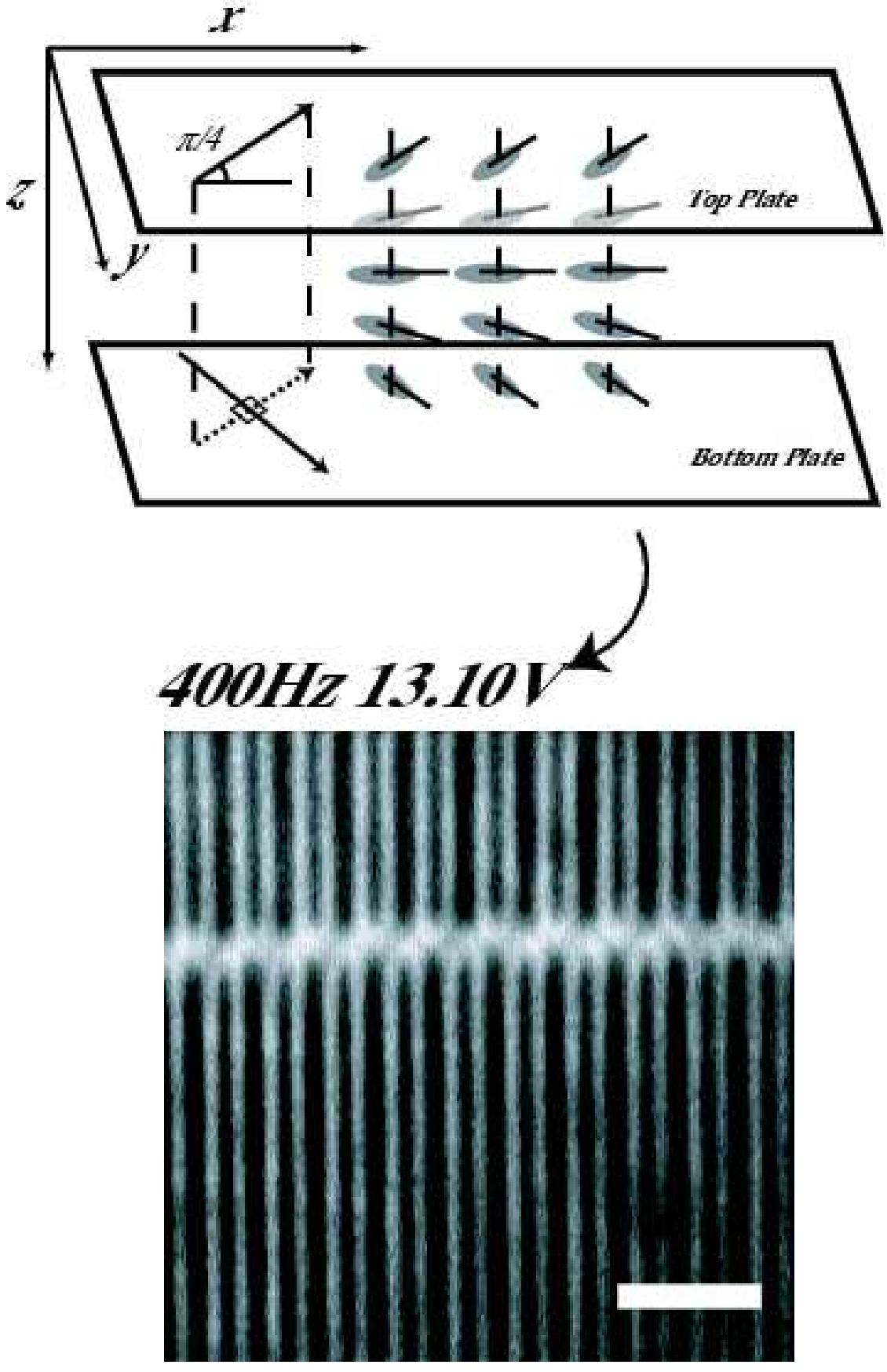


FIG. 1: Top: rubbing direction and the anchoring direction of nematic. Bottom: a typical phase jump line at 400Hz, 13.10 Volts. The white bar corresponds to 100$\mu m$.

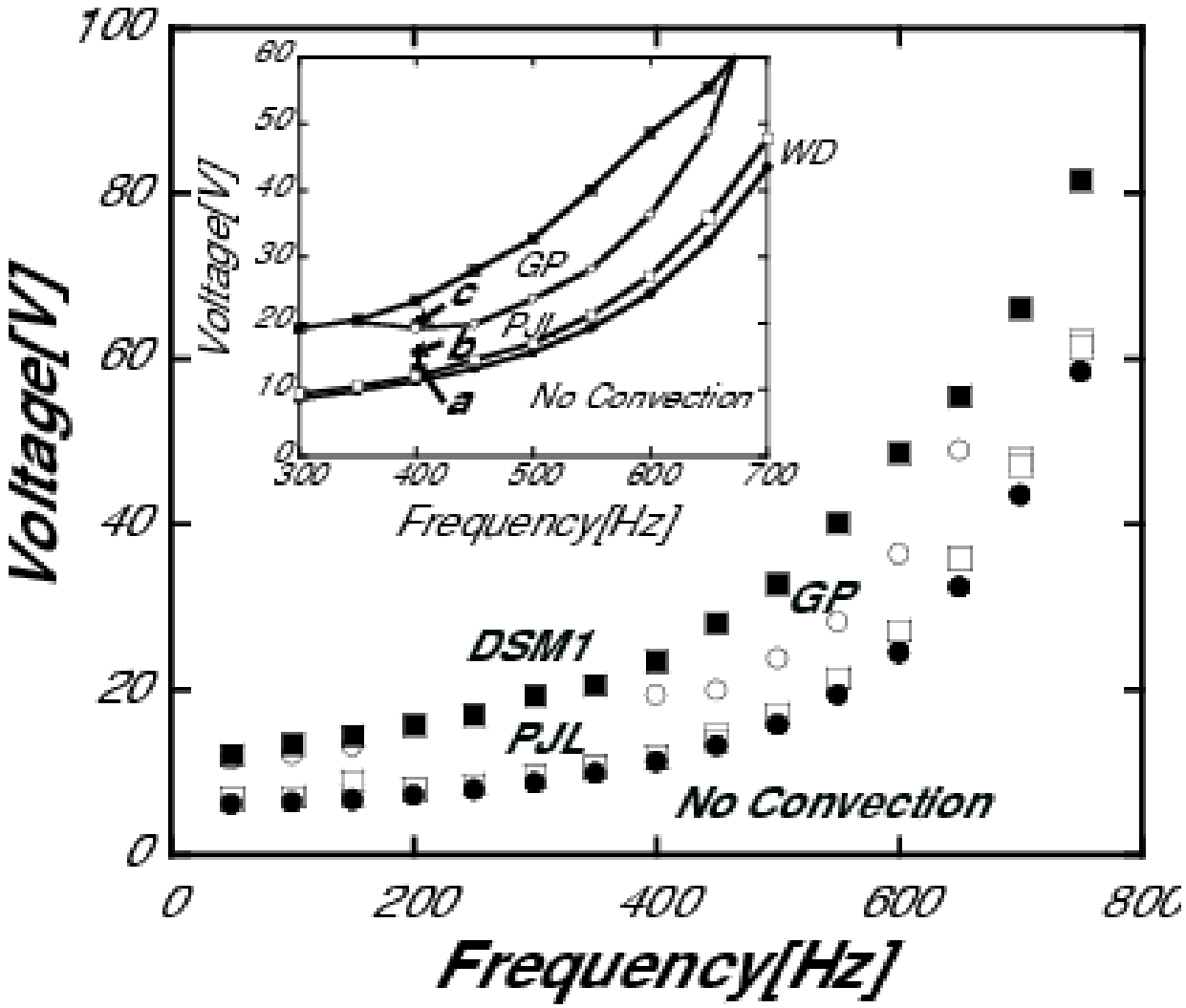


FIG. 2: Phase Diagram of our experiments. Solid circles represent the onset voltage of convection rolls (Williams Domain); open square the onset voltage of PJL; open circle represents the onset of the PJL grid pattern (GP); solid square the onset voltage of the dynamic scattering mode (DSM1). The inset shows the part of the phase diagram that we discuss in this paper. The points a, b and c in the inset correspond to Figs. 3a-c.

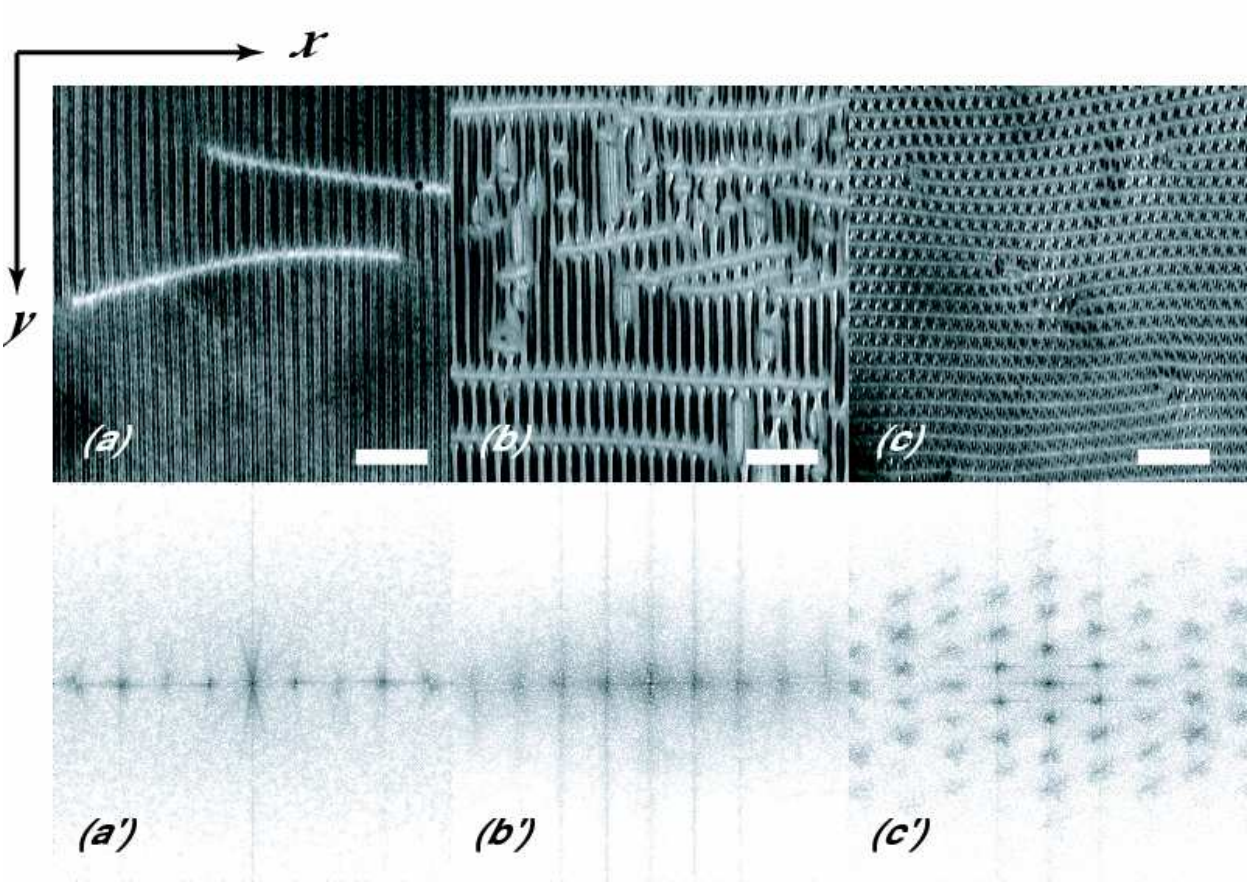


FIG. 3: The upper row shows images of convection patterns with PJL, the lower row the modulus of the corresponding 2D Fourier transforms. These three pair of figures represent the transition from PJL to GP. Fig. a corresponds to 13.93 V ($\epsilon = 0.47$), Fig. b to 15.91 V ($\epsilon = 0.91$), and Fig. c to 19.23 V ($\epsilon = 1.79$), all at 400 Hz. The length of the scale bars is $200\mu m$.

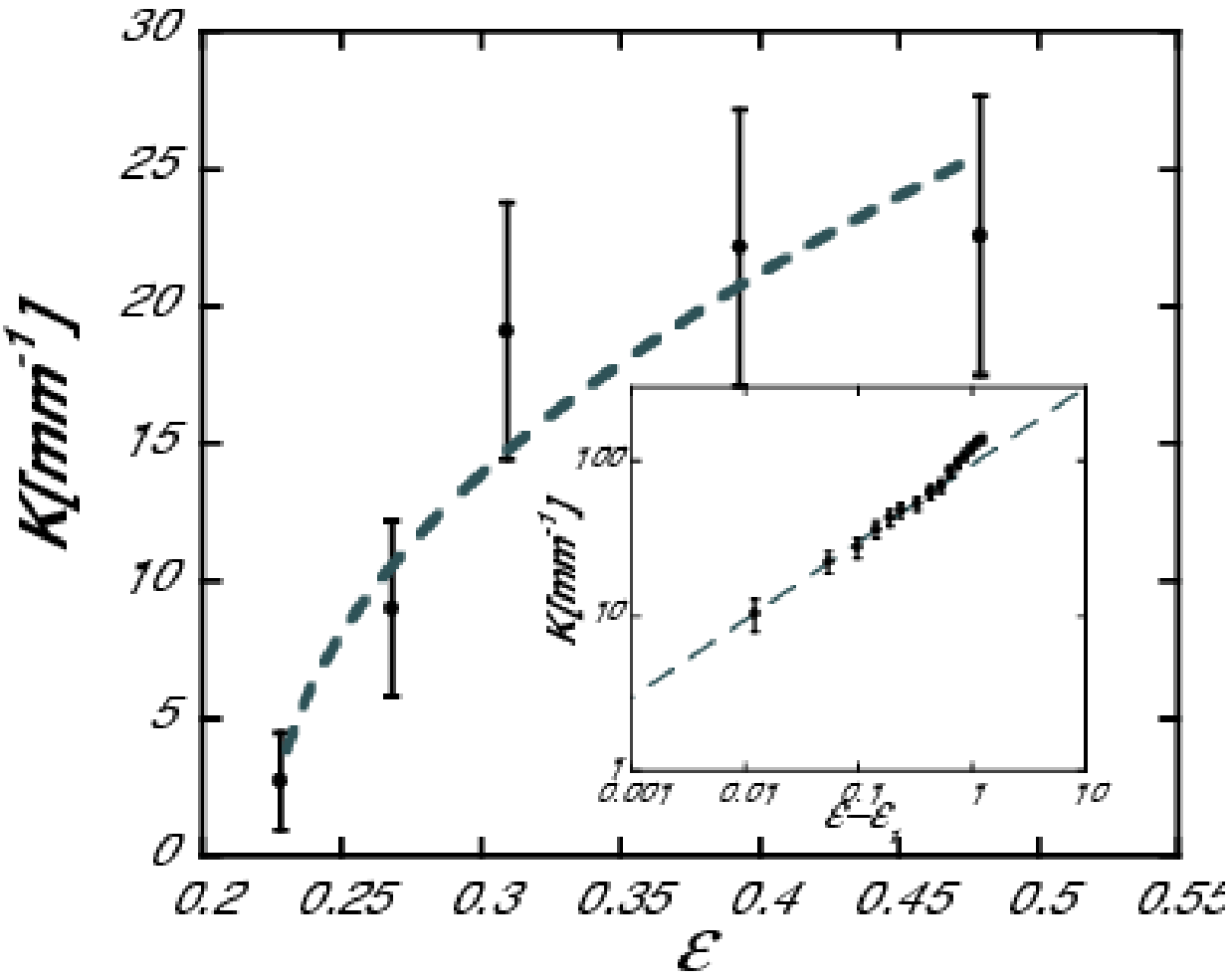
K[mm-1]
ε
K[mm-1]
ε−ε1

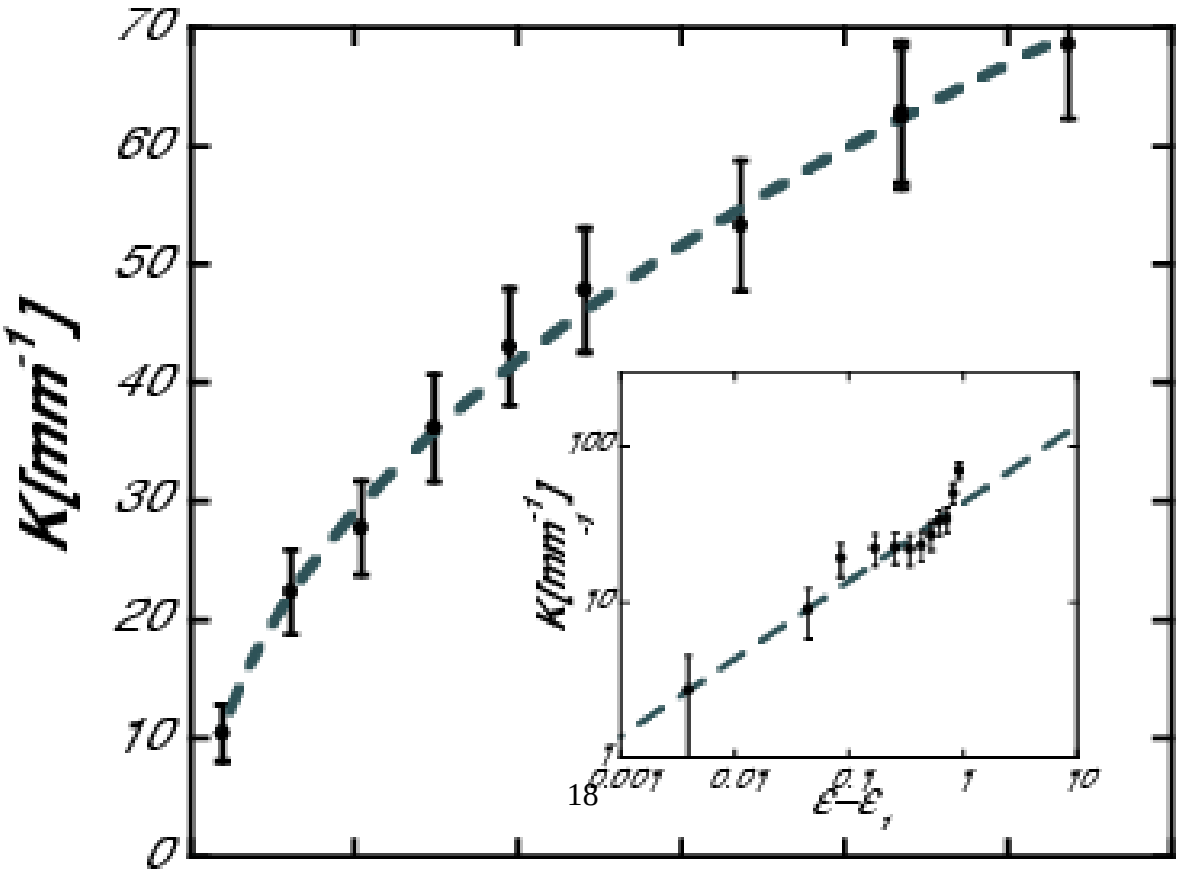
K[mm-1]
K[mm-1]
ε−ε1

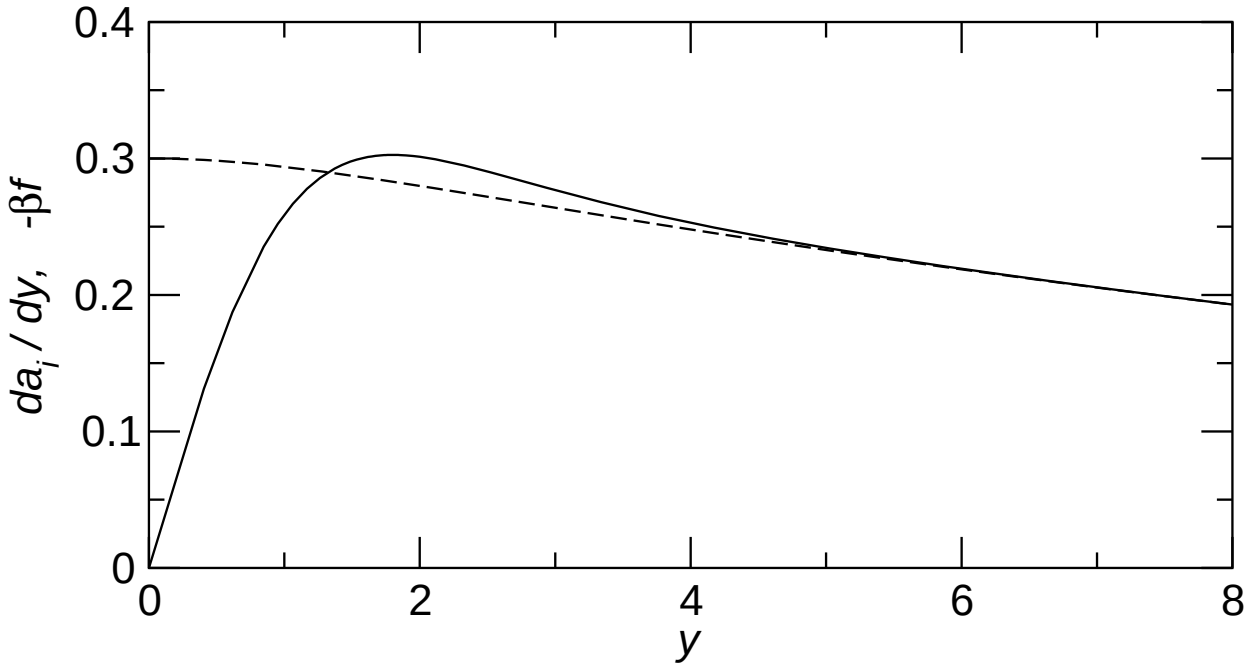


FIG. 5: Typical neutral mode of a phase jump line at the critical control parameter. Solid: $\partial_y a_i$, dashed: $-\beta f$.

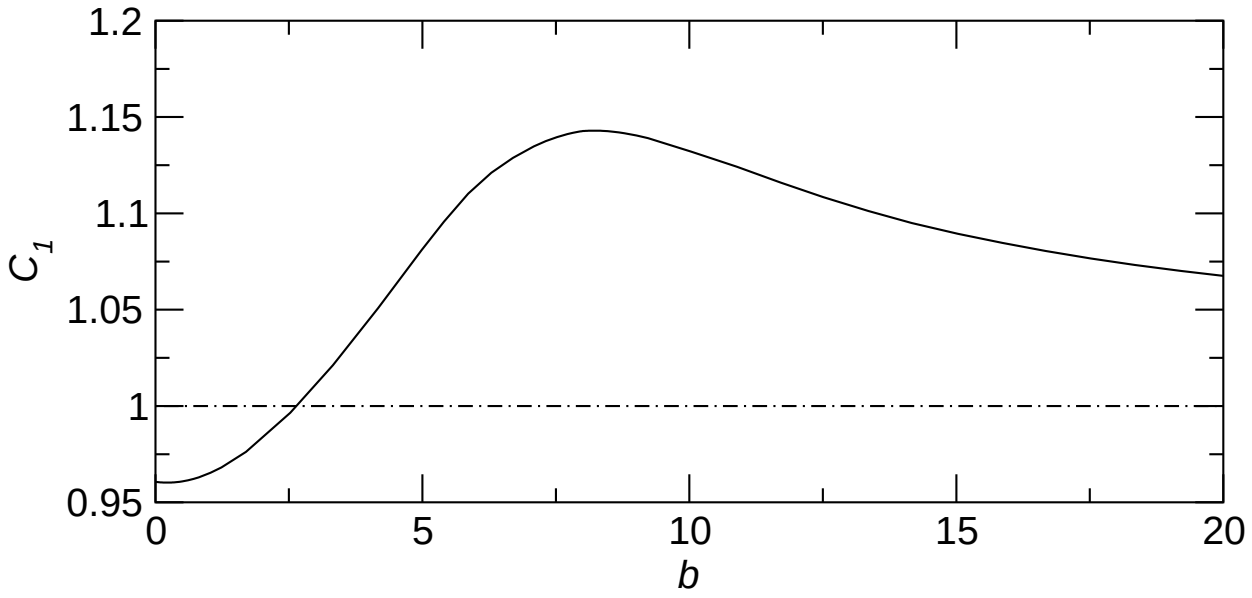


FIG. 6: The geometry factor $C_1$ in dependence of the twist $b$ for the simple model (14). The dash-dotted line at $C_1 = 1$ is a guide to the eye.